Urban Climate 43 (2022) 101157

Contents lists available at ScienceDirect

Urban Climate

journal homepage: www.elsevier.com/locate/uclim

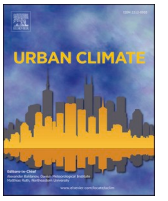

Vegetation cover change during a multi-year drought in Los Angeles

David L. Miller [a,b,*], Erin B. Wetherley [a], Dar A. Roberts [a], Christina L. Tague [c], Joseph P. McFadden [a]

[a] Department of Geography, University of California, Santa Barbara, CA 93106, United States
[b] Department of Environmental Science, Policy, and Management, University of California, Berkeley, CA 94720, United States
[c] Bren School of Environmental Science and Management, University of California, Santa Barbara, CA 93106, United States

ARTICLE INFO

Keywords:
Drought
California
Hyperspectral
Remote sensing
Land cover change
Urban forest

ABSTRACT

Vegetation in urban areas can provide many ecosystem services, such as cooler temperatures. In water-limited climates, maintaining benefits from vegetation during droughts requires significant water inputs and can be challenging due to the uneven effects of drought on vegetation. Here, we tracked changes in vegetation cover in Los Angeles, California using airborne hyperspectral imagery acquired annually from 2013 to 2018 and coinciding with the exceptional 2012–2016 California drought. Subpixel fractions for trees, turfgrass, non-photosynthetic vegetation (NPV; e.g., senesced plant material), and non-vegetated urban surfaces were mapped at 18 m spatial resolution using Multiple Endmember Spectral Mixture Analysis. We quantified cover changes through time, comparing how different physiographic regions of the city experienced vegetation change and assessing changes based on income and outdoor water use. From 2013 to 2018, overall turfgrass cover decreased (−17%) and NPV cover increased (+22%). Tree cover was more stable but decreased in 2018 (−6%). The inland valleys consistently lost more turfgrass than coastal areas. Higher income and water use areas had larger absolute changes in vegetation cover, likely due to their higher baseline of vegetation cover.

1. Introduction

Globally, many urban regions are projected to continue warming and drying under the influence of climate change (Zhao et al., 2021), resulting in many negative impacts for urban residents and the environment including heat stress, mortality, and increased energy demand which can spur further greenhouse gas emissions (Fraser et al., 2017; Hulley et al., 2019). Vegetation cover is able to ameliorate urban heat, and under future warmer temperatures and drier conditions its efficacy is projected to strengthen, with targeted increases in urban vegetation cover likely to mitigate the impacts of climate warming (Demuzere et al., 2014; Norton et al., 2015; Zhao et al., 2021). However, for cities in dry climates, this reduction in temperature often comes at the cost of large inputs of irrigation for vegetation (McPherson et al., 2011; Wheeler et al., 2019). This challenge can be exacerbated by drought, broadly defined as "a temporary reduction in water availability below normal quantities" (Lund et al., 2018), since drought can also diminish the effectiveness of vegetative evaporative cooling as vegetation becomes stressed, senesces, or is replaced (Winguth and Kelp, 2013;

* Corresponding author at: Department of Environmental Science, Policy, and Management, University of California, Berkeley, CA 94720, United States.
E-mail address: dlm@berkeley.edu (D.L. Miller).

https://doi.org/10.1016/j.uclim.2022.101157
Received 2 October 2021; Received in revised form 24 February 2022; Accepted 18 March 2022
Available online 23 March 2022

McPherson et al., 2018; Pincetl et al., 2019; Allen et al., 2021). Constraining these longer-term impacts of drought on heat reduction goals therefore requires quantifying vegetation cover changes, which will help better our understanding of planning requirements given future climatic conditions.

Across an urban region, the effects of drought on residents can be felt differently at local and neighborhood scales, primarily due to wide differences in the amount of vegetation cover and differences in drought responses among trees and turfgrass lawns. There are many physiological and environmental factors that can influence the response of trees to drought, such as tree species, leaf area, and the amount of surrounding impervious surface cover (May et al., 2013; Savi et al., 2015; Miller et al., 2020). At the same time, turfgrass lawns can senesce even at irrigation rates that are recommended to meet plant water demand due to high temperatures and high atmospheric demand for water during droughts (Chen et al., 2015; Quesnel et al., 2019). Extended, multiple-year droughts have the potential to magnify and enhance these effects, with potential for significant changes to the land cover and local urban climate (May et al., 2013; Pincetl et al., 2019).

During 2012–2016, California experienced one of the most severe droughts in the state's modern history, and many cities implemented urban water use restrictions to meet statewide reduction targets (Lund et al., 2018). Because these restrictions often limited irrigation and other outdoor water use, urban vegetation likely experienced reductions in water availability during this time period (Palazzo et al., 2017; Los Angeles Department of Water and Power, 2017; Pincetl et al., 2019). In semi-arid cities where planted vegetation requires urban irrigation, including many cities in southern California such as Los Angeles, trees and turfgrass lawns are especially likely to have distinct responses to long-term drought as irrigation restrictions are implemented (Bijoor et al., 2012; Mini et al., 2014; Litvak et al., 2017; Quesnel et al., 2019; Reyes et al., 2020; Allen et al., 2021). Trees can be deeply rooted and in the absence of irrigation may be able to obtain water from groundwater sources, even though many irrigated urban trees also have shallower roots and partly rely on surface irrigation of lawns, especially at high amounts of tree cover (Bijoor et al., 2012; Marchionni et al., 2021). Compared to turfgrass, trees are longer-lived, require years of investment and maintenance, and are not as readily replaced, and therefore their irrigation may be prioritized even when irrigation is restricted (Roman et al., 2018). In contrast, turfgrass lawns are more shallowly rooted and are likely to senesce rapidly under water limitation, but they also can be reinvigorated with subsequent irrigation and can regrow more easily (Kaufmann, 1994).

The differences between drought responses in urban trees and grass can also be affected by variations in climatological and physiographic conditions across an urban region, particularly in large cities with spatially extensive metropolitan areas (e.g., Allen et al., 2021). For example, the city of Los Angeles, California, has a strong coastal-to-inland gradient in climate (Tayyebi and Jenerette, 2016; Crum et al., 2017). Coastal areas have a more moderate climate, with cooler and wetter conditions, than areas in the inland valleys which are much warmer and drier, such as the San Fernando Valley to the north and the San Gabriel Valley to the east. Because of these climatic differences, the cooling effects of trees are more pronounced in the hotter inland regions (McPherson et al., 2011). There is also large topographic variability, with mountainous regions having lower urban development density than the flat areas in the basin and valleys. This can also influence solar exposure and, depending on the aspect the slopes, the intensity of drought conditions, which can be comparatively much more (south-facing) or less (north-facing) intense than other parts of the city with flatter topography.

In addition to differences by vegetation type and local climates, it remains unclear how the effects of a multi-year drought may differ based on the ability of residents to maintain existing vegetation cover in different areas of the city. In cities with dry climates, tree cover and overall vegetation abundance is often greater in areas having higher household income and/or higher irrigation water use (Schwarz et al., 2015; Palazzo et al., 2017). During an extended drought, higher income areas may be more buffered from vegetation losses due to their residents' ability to pay for irrigation water (Kaplan et al., 2014), and these areas are less likely to meet water conservation targets (Palazzo et al., 2017). Alternatively, these areas could experience greater absolute losses of vegetation as they generally have larger amounts of vegetated land that could be affected by drought in the first place (Schwarz et al., 2015). Lower income and lower water use areas may suffer smaller absolute losses of vegetation cover during drought because they have comparatively little vegetation to lose (Wolch et al., 2014; Tayyebi and Jenerette, 2016). Because of the high costs of landscape irrigation, the existing vegetation in lower income areas may be better acclimated to dry conditions experienced each year during the Mediterranean climate summertime drought, although people living in lower income areas are not necessarily more likely to plant more drought-tolerant tree species (Avolio et al., 2015). Nonetheless, an exceptional, long-term drought could push even nominally drought-tolerant vegetation beyond its normal limits (e.g., Miller et al., 2020), and more vegetation could be lost because people living in lower income areas would be less able to pay for additional outdoor water use (Palazzo et al., 2017).

The substantial spatial variation in drought responses given the heterogeneity of urban vegetation density and type (e.g., trees and turfgrass), metropolitan-scale climatic variability, and management practices can be quantified and mapped using remote sensing imagery. Although fine-scale urban spatial and spectral diversity can make it a challenge to distinguish among different urban land cover types (Herold et al., 2004; Cadenasso et al., 2007), a variety of data sources and methodological strategies have been developed in recent years to map urban tree cover or green vegetation cover. For tree cover mapping, many studies have used a combination of high spatial resolution imagery (e.g., Moskal et al., 2011; O'Neil-Dunne et al., 2014; Erker et al., 2019) and/or airborne LiDAR (e.g., Alonzo et al., 2014; Liu et al., 2017; Degerickx et al., 2020). Such studies tend to be limited to a single date and at relatively small spatial extent due to the expense of image acquisition and processing, making such data not suitable for studying drought impacts across a large metropolitan area. For larger spatial extents and longer time series, total green vegetation cover studies across larger areas often rely on broadband satellite imagery at coarser spatial resolutions (e.g., Richards et al., 2017; Czekajlo et al., 2020). These can provide estimates of the total green cover for many more dates due to regular satellite acquisitions, but they cannot often easily distinguish between different vegetation types unless other characteristics are included in the analysis (e.g., temporal patterns using phenology; Schug et al., 2020).

Hyperspectral sensors with hundreds of narrow spectral bands (i.e., imaging spectrometers) have been shown to more readily separate urban surfaces and vegetation types compared to broadband imagery (Herold et al., 2004; van der Linden et al., 2018). When applied to hyperspectral imagery, spectral unmixing techniques such as Multiple Endmember Spectral Mixture Analysis (MESMA; Roberts et al., 1998) have been used to successfully distinguish subpixel fractions of urban surfaces, including separating tree and turfgrass cover (e.g., Herold et al., 2004; Franke et al., 2009; Wetherley et al., 2017; Wetherley et al., 2018). Hyperspectral imagery can also capture the spectral detail necessary to distinguish non-photosynthetic vegetation (NPV; e.g., senesced grass, plant litter) from soil and other non-vegetated surfaces, which is often infeasible using broadband imagery (Wetherley et al., 2017). This distinction is important because while dieback from green vegetation to NPV is indicative of drought effects (Dennison et al., 2019), it is also evidence of the persistence of vegetation cover through a drought as opposed to conversion to another type of non-vegetated urban surface (e.g., Pincetl et al., 2019).

The application of hyperspectral imagery for extensive urban studies through time has been limited, mainly because such imagery has rarely been available in urban areas over large areas and typically only for a single date. However, the NASA HyspIRI Preparatory Campaign (Lee et al., 2015) acquired repeat flights across many regions in California using the Airborne Visible Infrared Imaging Spectrometer (AVIRIS; Green et al., 1998) as a test-case for a future spaceborne hyperspectral sensor, the now-planned Surface Biology and Geology mission (SBG; Cawse-Nicholson et al., 2021). In the Los Angeles area, HyspIRI Preparatory Campaign imagery were acquired at several dates throughout the year from 2013 to 2015 and then at a single date each year from 2016 to 2018. This provides an unprecedented opportunity to track an annual drought time series in an urban area using hyperspectral imagery, and this type of analysis may become more common when imagery from future spaceborne hyperspectral monitoring instruments becomes available in the next few years.

Quantifying the drought-induced changes in urban vegetation cover will be critical for urban planning for heat mitigation and

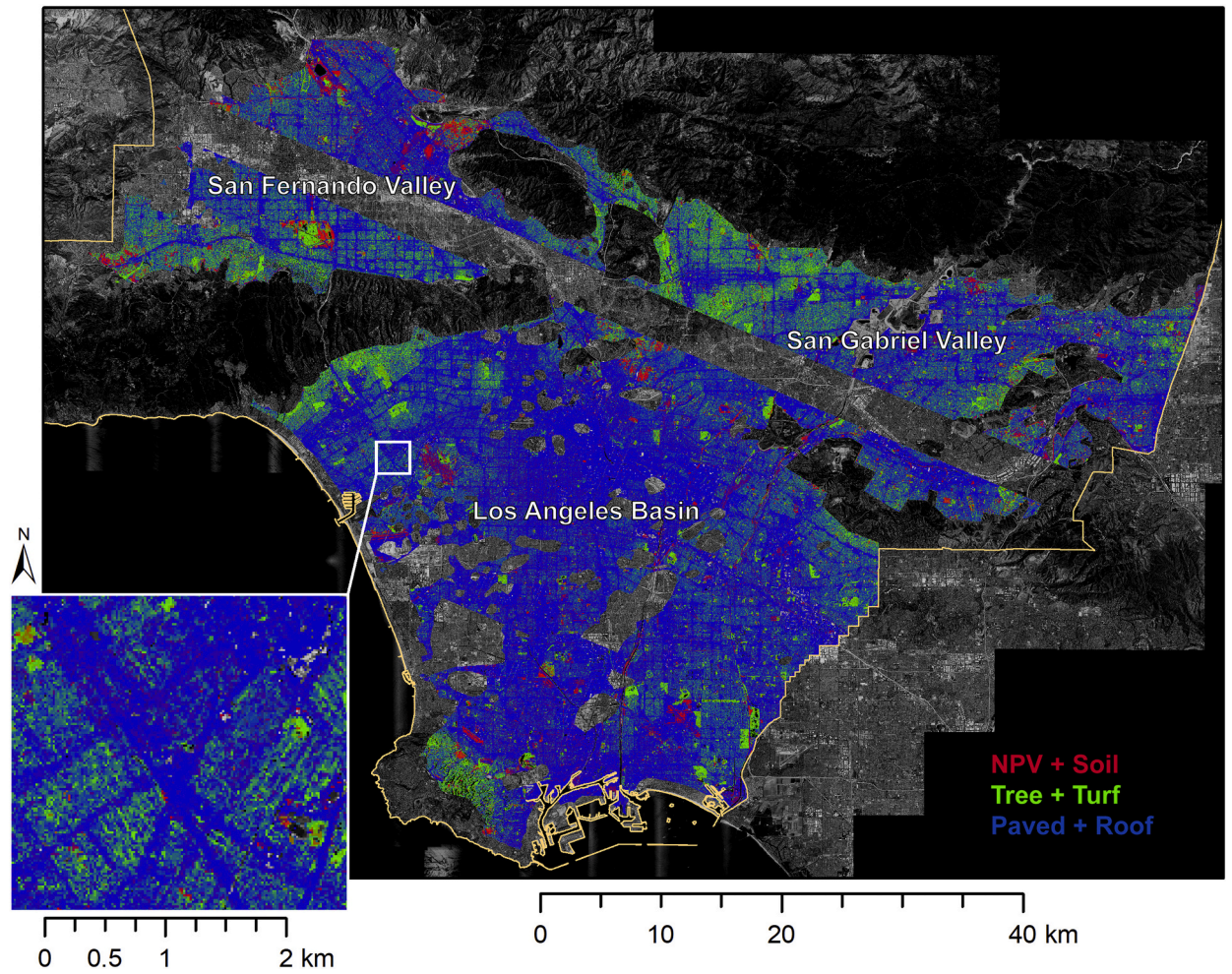

Fig. 1. Map of fractional cover on 22 May 2013 within the Los Angeles urban study area. Background is grayscale National Agricultural Inventory Program (NAIP) aerial photo mosaic and Los Angeles County outline is in light orange. Example inset on lower left (near Culver City) shows detail of 18 m imagery. Missing areas are primarily due to masked clouds, removed undeveloped and agricultural areas, and other image artifacts (e.g., diagonal section in northern part of study area).

adaptation as the likelihood of extreme droughts is projected to increase with climate change (Norton et al., 2015; Williams et al., 2015; Zhao et al., 2021). Separately tracking trees, turfgrass, and NPV is especially needed for monitoring vegetation response during drought, because while some areas may experience temporary changes from green vegetation cover to NPV and have the potential to green-up once water is available, other areas may experience replacement of green vegetation with impervious surfaces and/or xeriscaping (Pincetl et al., 2019). These differences can have profound effects on energy budgets and water use, and they can modify the aesthetic characteristics and amenities of the urban environment in ways that would likely continue long after the end of the drought (Liang et al., 2017; Pincetl et al., 2019; Wetherley et al., 2021).

Here, we track changes in different types of vegetation cover across the Los Angeles metropolitan area during a multi-year drought. Specifically, we used late spring / early summer hyperspectral remote sensing imagery at 18 m spatial resolution as drought conditions progressed from 2013 to 2018 (US Drought Monitor, 2020). Subpixel fractions of tree, turfgrass, NPV, and non-vegetated surfaces (e.g., pavement, roofs, and soils) were calculated using MESMA. We focused our analysis on the following research questions:

1. In response to a historic multi-year drought, how did urban tree, turfgrass, and NPV cover in Los Angeles change year-to-year during 2013 to 2018?
2. In which climatological and physiographic regions of the city were vegetation changes most pronounced?
3. Using household income and outdoor water use as proxies, how did changes in vegetation cover types vary based on ability of residents to maintain their vegetation cover?

2. Methods

2.1. Los Angeles study area

Our study area was the Los Angeles metropolitan area (hereafter referred to as “Los Angeles”) in southern California, USA, including the city of Los Angeles and surrounding cities in Los Angeles County (2490 km^2; 34.05° N, 118.25° W; Fig. 1). Study area boundaries were based on urbanized area extent from the US Census Bureau (2010), manually edited to remove undeveloped and agricultural regions along the margins (Wetherley et al., 2018), and then limited to the boundaries of Los Angeles County. Los Angeles County has a population of 10 million (US Census Bureau, 2020) and the Los Angeles metropolitan area is characterized by expansive low-rise suburban development (Davis, 2006). It has a Mediterranean climate with wet winters and dry summers (Los Angeles downtown mean annual precipitation = 37.9 cm, mean annual air temperature = 18.6 °C; (National Centers for Environmental Information, 2020). A strong coastal climate gradient spans the area, generating comparatively cooler and wetter conditions near the Pacific Ocean and warmer and drier areas in the inland valleys.

As opposed to cities in wetter climates, increases in urban tree cover in the Los Angeles region are a direct result of the city’s development (Gillespie et al., 2012). Because of its climate, the Los Angeles region did not have extensive tree cover prior to urbanization (except for agricultural orchards), instead being dominated by coastal sage scrub and chaparral with comparatively few trees along riparian corridors (Pincetl et al., 2013b). In general, the city of Los Angeles has increased in tree canopy cover and stem density as urban development increased over the 20th century, although with wide variability in different parts of the city (Gillespie et al., 2012) and under the influence of different tree planting programs (Pincetl et al., 2013a). The combination of a mild climate and extensive irrigation allows for a highly diverse number of tree species in the urban forest, with over 200 species estimated throughout the city (Clarke et al., 2013). Different areas of the metropolitan region also may show differences in urban forest diversity because of changes in the tree species that were available to buy from nurseries at the time period when each area was developed, with relatively few native trees in the overall urban forest species palette (Pincetl et al., 2013b; Avolio et al., 2015).

The Los Angeles metropolitan area experienced severe drought from 2012 to 2019, with nearly the entire urbanized region experiencing exceptional drought conditions from mid-2014 to the beginning of 2017 (Table 1, US Drought Monitor, 2020). The first year in our time series during which HyspIRI Preparatory Campaign flights were available (2013) was already during the drought. Drought persisted across nearly all dates of image acquisition (2013–2018) based on drought indices derived from precipitation and

Table 1
AVIRIS image dates and related drought information. Drought Severity and Coverage Index (DSCI; no drought = 0, maximum drought = 500) values are from the US Census Bureau (2010) for the Los Angeles-Long Beach-Anaheim, CA urban area from nearest available dates. The Palmer Drought Severity Index (PDSI), 6-month estimates of the Standardized Precipitation Evapotranspiration Index (SPEI), and 6-month precipitation totals (ending in the month of each image date) are from the US Historical Climate Network Station in Pasadena, California (Abatzoglou et al., 2017). Both PDSI and SPEI values are normalized such that positive values are associated with wetter conditions and negative values are associated with drier conditions. The column “Precip. (% of average)” refers to the amount of rainfall during the previous 6 months (“Precip. (cm)”) compared to long-term climatology (1981–2010) for the study area.

AVIRIS image date	DSCI	PDSI	SPEI	Precip. (cm)	Precip. (% of average)
22 May 2013	200	−4.68	−1.43	19.5	42.3
13 June 2014	400	−6.56	−1.49	15.3	38.6
28 May 2015	496	−3.95	−0.46	35.8	77.8
16 June 2016	496	−2.85	−0.73	26.1	65.6
28 June 2017	129	−2.18	0.19	40.0	100.6
25 June 2018	300	−4.87	−0.88	20.7	52.0

evapotranspiration (Abatzoglou et al., 2017; US Drought Monitor, 2020), including the Palmer Drought Severity Index (PDSI; Palmer, 1965) and the 6-month Standardized Precipitation-Evapotranspiration Index (SPEI; Vicente-Serrano et al., 2010). Although urban vegetation likely responded to seasonal variations in drought severity (e.g., in nearby Santa Barbara, California; Miller et al., 2022), at the annual scale, the years of 2013–2016 were successive years of continuous drought. 2014 was the most severe single drought year. 2017 had nearly average rainfall, and 2018 saw a return to moderate drought conditions (Table 1). In response to dry conditions, the City of Los Angeles implemented a variety of water conservation measures, largely focused on outdoor water use because that was found to be the area with the most reduction potential, including: higher rebate rates for turfgrass lawn replacement, a new water rate-tiering structure, "Unreasonable Water Use" restrictions and fines for very high water users, and greater investment in education and outreach campaigns (Los Angeles Department of Water and Power, 2017).

2.2. Hyperspectral remote sensing time series

To track multi-year vegetation canopy changes, we used a repeat time series of hyperspectral imagery from the Airborne Visible Infrared Imaging Spectrometer (AVIRIS), which measures 224 narrow bands of spectral radiance from approximately 360 to 2500 nm at 10 nm full-width half-maximum (Green et al., 1998). We selected seven adjacent flightlines collected as part of the Southern California Box of the HyspIRI Preparatory Campaign (Lee et al., 2015) flown on an ER-2 aircraft at 20 km altitude in May/June of 2013–2018 (Table 1). Available data for all years of the time series were limited to early summer acquisitions; however, this provided good phenological timing, with deciduous trees having leafed out and drought-affected vegetation senescing due to lack of irrigation, particularly if winter and spring precipitation was poor (Avolio et al., 2015; Litvak et al., 2017; Miller et al., 2022). The flightlines were atmospherically corrected to Level 2 surface reflectance products produced by NASA Jet Propulsion Laboratory (JPL; Thompson et al., 2015). Each flightline was spatially coregistered to an 18 m grid using nearest neighbor resampling with Delaunay triangulation; up to 40 ground control points per line (supplemental material, Table S1) were developed using pixel-aggregated National Agricultural Inventory Program color-infrared orthophotos (NAD 83, UTM Zone 11 N) as a base image.

Although all images were produced to satisfactory surface reflectance by JPL, images from different years were generated using slightly different atmospheric correction processes. To improve internal consistency in surface reflectance retrievals, we calibrated each set of atmospherically corrected imagery to the AVIRIS imagery from 28 August 2014 used in Wetherley et al. (2018). Following Wetherley et al. (2018), we normalized each flightline using in-scene temporally invariant targets (i.e., a large parking lot and a bare soil field) to develop band-by-band calibration coefficients (supplemental material, Figs. S1–S4). Clouds and cloud shadows were masked manually from all dates. While inspecting the data, the brightness of the northern edge of one flightline (FL06) was observed to be inconsistent with all other flightlines, and this part of the flightline was removed from analysis. Imagery within each date of acquisition was mosaicked, and all remaining bands with apparent atmospheric artifacts removed, leaving 168 bands for analysis.

2.3. Generating subpixel land cover fractions using MESMA

We produced maps of subpixel fractional cover following Wetherley et al. (2018), using Multiple Endmember Spectral Mixture Analysis (MESMA; Roberts et al., 1998) in Viper Tools 2.1 (Roberts et al., 2019). Briefly, MESMA uses a library of known spectral endmembers (e.g., trees, turfgrass, constructed materials) to estimate the fractional cover within each measured pixel spectrum. It models each measured pixel spectrum as a linear combination of spectral endmembers, selecting the best model based on the smallest RMSE, and can vary the number and specific endmembers used for each pixel (Roberts et al., 1998). In this study, the fractional cover estimates were derived from a spectral library developed by Wetherley et al. (2018) from AVIRIS imagery acquired in August 2014 in the Los Angeles area. Image endmembers included trees, turfgrass, NPV, soil, paved surfaces, and commercial roofs. We modeled non-vegetated surfaces separately (i.e., soil, paved surfaces, and commercial roofs) instead of as a single class because it increased the number of successfully modeled pixels. We refer to Wetherley et al. (2018) for details regarding spectral library endmember selection and curation to a final set of 57 endmembers: 8 tree, 6 turfgrass, 9 pavements, 22 commercial roofs, 7 NPV, and 5 soils. Wetherley et al. (2018) validated fractions derived from this spectral library for their August 2014 imagery, and linear regressions with reference estimates had slopes from 0.77 to 0.90, depending on the cover type. We estimated subpixel fractions as 1, 2, or 3 endmember models plus shade (for spectral brightness normalization) using physically realistic fraction limits (0.00 to 1.00), a maximum shade endmember fraction of 0.20, and RMSE $\leq$2.5%, with a more complicated model only being selected if RMSE was improved by $\geq$0.7%. All fraction estimates were shade normalized so that the sum of all subpixel fractions was 1 (Dennison and Roberts, 2003). To retain the same sample of pixels through time, areas of cloud masking and unmodeled pixels (complexity = 0) were propagated across all image dates and were excluded from analysis.

2.4. Ancillary data and statistical assessment

2.4.1. Total year-to-year changes in cover among vegetation types

We analyzed temporal changes in vegetation cover, tracking changes in the fractional cover of trees, turfgrass, NPV, and non-vegetated surfaces (i.e., sum of pavement, roofs, and soil). We estimated mean fractional cover (i.e., land cover in each pixel sums to 1) for the entire study area for each year. Since the cover fractions for individual pixels were not normally distributed (i.e., many values stacked at fractions of 0 and 1) and could not be tracked pairwise through time, we used US census tracts as the unit of analysis to evaluate temporal variability in cover type distributions (US Census Bureau, 2010; County of Los Angeles, 2020). To assess the relationship between vegetation type composition and total vegetation abundance, we also compared the proportional cover of trees,

turfgrass, and NPV within census tracts as the total combined vegetation cover increased. In order to estimate the heterogeneity of change, we calculated the standard deviation of mean values across all census tracts, weighted by the number of pixels extracted within each census tract.

2.4.2. Vegetation cover changes in different physiographic regions of the city

To visualize and map the cumulative changes across the study area from 2013 to 2018, we aggregated mean cover estimates by census tracts that contained at least 50 pixels (of any cover type, vegetated or non-vegetated), taking the difference from 2013 and 2018 vegetation cover estimates (i.e., trees, turfgrass, or NPV). Change in each census tract was displayed on a map of the study area from which we could evaluate how vegetation types in different regions of the city changed through time.

2.4.3. Vegetation cover changes based on household income and outdoor water use

To evaluate vegetation cover changes during the drought across areas of the city that differed in median household income and estimated outdoor water use, we used US Census Bureau income data and water use data from an average rainfall year (2006). Although income and landscape irrigation volume are strongly correlated in Los Angeles ($R = 0.71$; Mini et al., 2014), we wanted to evaluate vegetation cover changes from independent sources at different spatial scales. This allowed us to broadly characterize the effect of affluence and the likely ability of different neighborhoods to maintain green vegetation throughout the drought. Polygons for median household income in 2018 were organized at the census tract scale (mean area = 1.20 km^2, SD = 1.12 km^2) across the entire study domain within Los Angeles County, while the outdoor water use data were estimated from postal carrier route polygons (mean area = 0.40 km^2; SD = 0.28 km^2) within the City of Los Angeles. This meant that the income census tract polygons were more appropriate for overall neighborhood-scale analysis across a broader domain of the urban area, whereas the water use polygons were more sensitive to changes in single-family residential areas.

Median household incomes for 2018, aggregated for each 2010 census tract from the American Community Survey, were retrieved from the Los Angeles County data portal (County of Los Angeles, 2020). We stratified the income levels based on a bin width of $30,000 up to a level of $120,000, with values >$120,000 in a single bin. Across these income levels, we compared distributions in surface cover throughout the drought and changes in tree, turfgrass, and NPV cover types. Weighted mean values across census tracts were used to calculate standard deviations for cover type changes by income level.

Vegetation change within areas of different irrigation regimes were calculated using estimates of outdoor water use extracted from single-family residential water use data aggregated to postal carrier route polygons within the City of Los Angeles (Chen et al., 2015). Data for the 2013–2018 study time period of were not available, but as a means of stratifying different areas of the city by water use patterns, we relied on available water use data from 2006, an average rainfall year. This allowed us to compare vegetation change in different parts of the city that characteristically have differing levels of outdoor water use. Postal carrier route polygons with large golf courses were removed from analysis, and we included only polygons containing at least 50 image pixels.

For each postal carrier route, we estimated average single-family residential outdoor water use per household (m^3 / household). We estimated outdoor water use per household, instead of per unit area, because we were interested in how well vegetation was retained during the drought based on total outdoor water use irrespective of property size. Note that we are using outdoor water use here as an indication of a household's capacity to maintain vegetation rather than analyzing irrigation efficiency using relationships between vegetation greenness and irrigation intensity. Water use data were available as sums for each postal carrier route, and we divided the sums by the number of single-family households in each carrier route to estimate water use per household. Outdoor water use per household for each postal carrier route was estimated by calculating the difference in water use between February and June, following Chen et al. (2015) and Wetherley et al. (2018). This assumes that February, the wettest month of the year, is the least irrigated and is thus a proxy for calculating indoor water use. Subtracting this amount from water use in June, corresponding to the most common month of imagery used in this study, results in an estimate of outdoor water use. This is likely a minimum estimate for outdoor water use since outdoor irrigation also occurs in February in the study area, and true outdoor water use may in fact be higher (Chen et al., 2015). The few postal carrier route polygons that violated this assumption (i.e., had lower water use in June compared to February) were removed from analysis ($n = 8$). Similar to the error estimation for income, weighted mean values across postal carrier routes were used to calculate standard deviations for cover type changes by water use level.

To compare temporal changes in vegetation based on both income and outdoor water use, we used two main methods: absolute and relative change. In both cases, we compared changes for trees, turfgrass, and NPV relative to the mean of the time series to assess year-to-year adjustments. First, we compared changes in terms of absolute fractional cover, meaning the raw fractional estimates (0 to 1) retrieved for different levels of income or outdoor water use. This summarized where the largest changes in vegetation cover occurred in the city. Second, we compared percent changes relative to the mean of the time series, because of the large differences in the baseline amounts of vegetation cover for the different income and outdoor water use levels (Mini et al., 2014; Tayyebi and Jenerette, 2016). This second method was to normalize for a fairer comparison across different income and outdoor water use levels.

3. Results

3.1. Overall vegetation changes during the drought

Overall land cover was assessed across the full study area. We report all mapped fractions and their absolute change estimates as a decimal value (i.e., 0 to 1), and all estimates of relative percent change in fractions from the mean of the time series as a percentage (e.g., +10%). During the study period, non-vegetated surfaces were the dominant form of cover overall, composing a mean fractional

cover across all dates of 0.709 of the area. Trees were the dominant form of vegetation cover (mean = 0.195), with turfgrass at a mean of 0.035 and NPV at a mean of 0.062 fractional cover (Table 2).

To gauge overall changes during the drought, the mean cover for each cover type across all dates (shown on the last row in Table 2) was used as a benchmark against which annual changes were assessed as percent change anomaly (Fig. 2). Generally, cover fluctuated throughout the study period, with overall losses in turfgrass cover, increases in NPV, and relatively stable tree cover until losses were detected in 2018. Turfgrass cover exhibited annual decreases from its high in 2013, with the exception of a significant green up event following higher winter rains in 2017. NPV had low values in 2013, 2014, and 2015, but had higher values in 2016 and 2018. At the end of the time series in 2018, trees and turfgrass had their lowest mean values and NPV had its highest mean values. Considerable heterogeneity in change was observed across individual census tracts, with one standard deviation from the mean change always overlapping the mean of the time series (i.e., zero change value).

When aggregated to census tracts, the proportions of vegetation cover types were different based on the amount of total vegetation cover (i.e., tree + turfgrass + NPV), but these proportions were mostly stable during the drought time series (Fig. 3). In general, census tracts with low total vegetation cover (<0.25) had relatively fewer trees and more NPV in their vegetated areas than did census tracts with higher total vegetation cover. The proportions of tree, turfgrass, and NPV cover stayed relatively consistent for census tracts having >0.3 total vegetation cover. Census tracts with very high overall vegetation cover (> 0.6) were more variable year to year. Although these proportions did not undergo large changes through time, the proportion of tree cover decreased and NPV cover increased from 2013 to 2018 for census tracts having total vegetation fractional cover between 0.3 and 0.5.

Mean tree and turfgrass cover decreased and NPV cover increased from 2013 to 2018 (Table 2), but the nature of the change varied across different regions of the study area (Fig. 4):

1. Turfgrass loss was more extensive farther from the coast in the inland valleys, with the greatest losses occurring north and east of the Los Angeles Basin in the San Fernando and San Gabriel Valleys (Fig. 4A). Additional large losses of turfgrass cover occurred in the highly vegetated foothill areas at the perimeter of the Los Angeles Basin (e.g., Beverly Hills, Rancho Palos Verdes, Whittier). By contrast, turfgrass cover appeared to increase south of downtown Los Angeles in residential areas and commercial districts (e.g., Vernon) as well as closer to the ocean in the west (e.g., Santa Monica, Torrance).
2. Overall spatial changes in tree cover were not as apparent as they were in turfgrass, but from 2013 to 2018 more areas experienced tree cover losses than gains (Fig. 4B). The tree cover losses were scattered throughout the Los Angeles Basin, as well as to the north and east in the San Fernando and San Gabriel Valleys. Tree cover fraction increased in the southwest of the San Fernando Valley (e.g., Woodland Hills), and as well as the northwest (e.g., UCLA) and east (e.g., Whittier) of the Los Angeles Basin.
3. The spatial patterns of overall green vegetation (tree + turfgrass) cover changes (Fig. 4C) were more similar to changes in turfgrass rather than tree cover.
4. Fig. 4D shows that total vegetation cover (tree + turfgrass + NPV) was lost in the inland valleys, most strongly in the San Gabriel Valley, but increased in many parts of the Los Angeles Basin. This is because increases in NPV were often apparent in areas that also lost turfgrass cover, such as in the San Fernando Valley and the hills to the south of the San Gabriel Valley (Fig. 4E). However, NPV cover decreased in some areas where turfgrass increased, such as south of downtown Los Angeles. Notably, turfgrass losses in the San Gabriel Valley itself did not lead to as large increases in NPV proportionally as might have been expected, suggesting that this region may have experienced more conversion from turfgrass to non-vegetated urban surfaces than other areas.

(Larger versions of difference maps in Fig. 4 showing anomalies between 2013 and 2018, as well as differences between the mean of the time series and 2018, are provided in the supplemental material, Figs. S5–S14.)

3.2. Vegetation change related to income and water use

3.2.1. Income

We compared changes in vegetation cover based on absolute fractional cover for different levels of median household income (Fig. 5A). For most income levels, tree cover was lowest in 2018 but did not consistently decrease year-over-year as the drought progressed. Higher income levels generally had greater shifts in yearly mean tree cover than lower income levels. Turfgrass had a more

Table 2
Mean fractional cover of the major urban vegetation types for each year across the entire study area. NPV is non-photosynthetic vegetation (e.g., senesced grass, plant litter) and NON-VEG includes pavement, roofs, and bare soil. Standard deviation (SD, in parentheses) is calculated from the means of census tracts ($n = 1935$), weighted by number of available pixels within each census tract. All years had below average winter rainfall except for 2017, which had average rainfall for the study area.

Year	TREE	TURF	TREE + TURF	NPV	TREE + TURF + NPV	NON-VEG
2013	0.194 (0.109)	0.036 (0.029)	0.231 (0.124)	0.058 (0.042)	0.289 (0.134)	0.711 (0.134)
2014	0.205 (0.103)	0.034 (0.033)	0.239 (0.119)	0.060 (0.044)	0.300 (0.133)	0.700 (0.133)
2015	0.196 (0.103)	0.033 (0.028)	0.229 (0.118)	0.057 (0.042)	0.285 (0.131)	0.715 (0.131)
2016	0.193 (0.097)	0.031 (0.029)	0.224 (0.111)	0.067 (0.046)	0.290 (0.127)	0.710 (0.127)
2017	0.198 (0.095)	0.039 (0.035)	0.237 (0.112)	0.062 (0.048)	0.299 (0.132)	0.701 (0.132)
2018	0.183 (0.095)	0.030 (0.028)	0.213 (0.110)	0.071 (0.047)	0.284 (0.126)	0.716 (0.126)
Mean	0.195 (0.101)	0.034 (0.030)	0.229 (0.116)	0.062 (0.045)	0.291 (0.131)	0.709 (0.131)

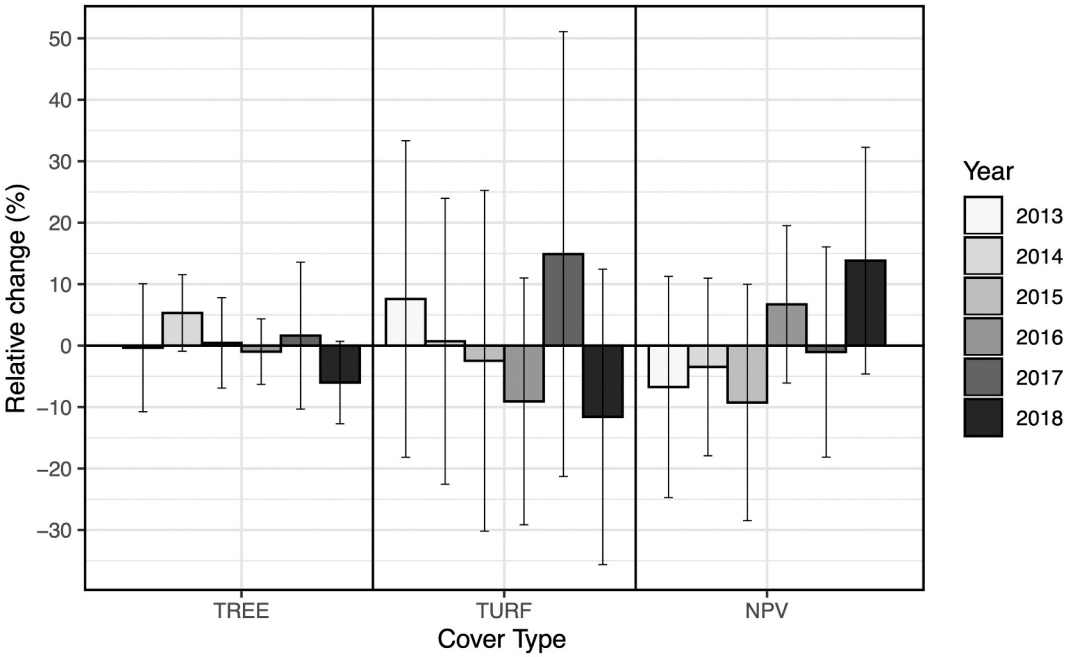

Fig. 2. Annual mean percent change (2013–2018) anomalies of fractional cover from the mean of the time series for the full study area for trees, turfgrass lawns, and NPV. Error bars show ±1 SD based on weighted means of census tracts. While other years were drier than normal, 2017 was an average rainfall year.

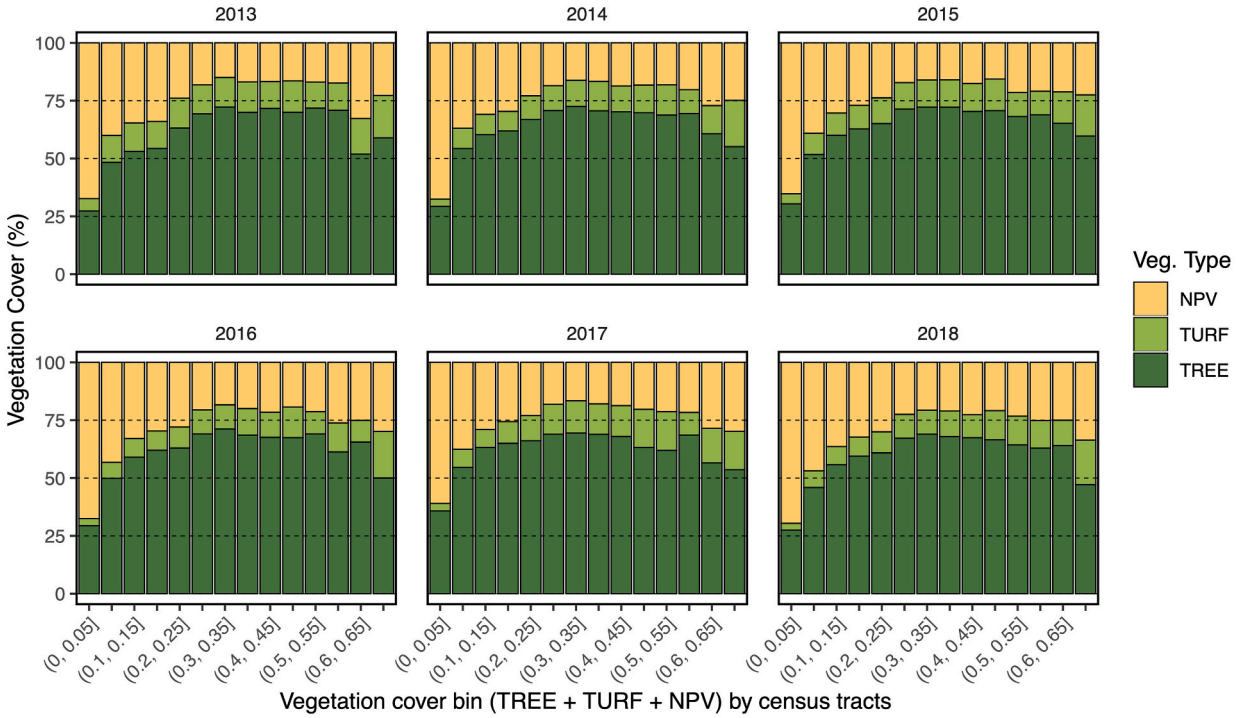

Fig. 3. Annual distributions of vegetation cover types within bins of total vegetation cover (tree + turfgrass + NPV) as aggregated to mean fractional cover within census tracts.

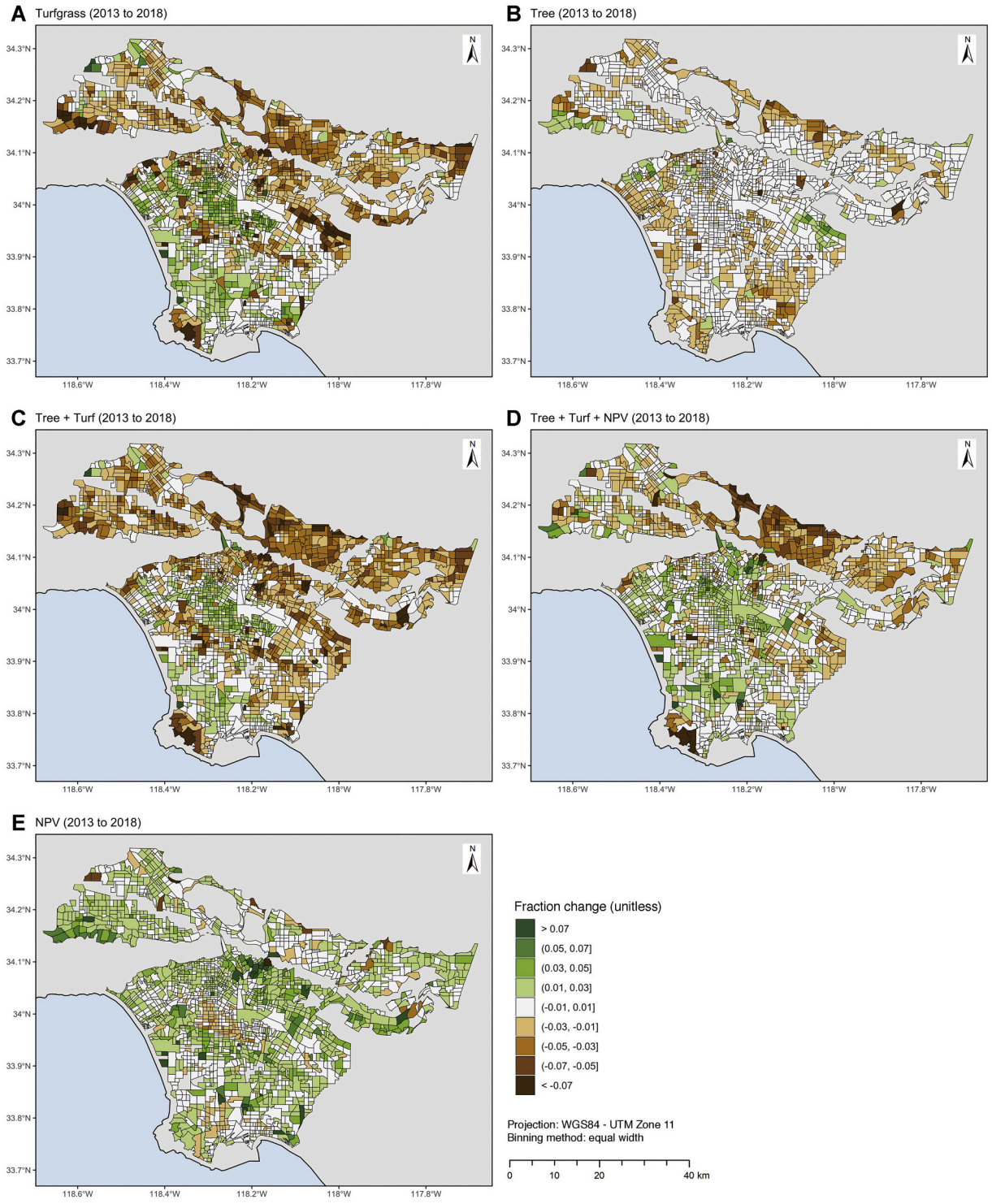

Fig. 4. Mean cumulative changes in vegetation cover fractions from 2013 to 2018 by census tracts for: (A) turfgrass; (B) tree; (C) tree + turfgrass, i.e., overall green vegetation cover; (D) tree + turfgrass + NPV, i.e., total vegetation cover; and (E) NPV, i.e., senesced vegetation, dead grass, plant litter. For each map (UTM zone 11, datum WGS84), green colors represent increases and brown colors represent decreases for each vegetation cover type within each census tract (fraction change is unitless, m^2 / m^2). Bins are of equal width, with the exception of the maximum and minimum bins. Census tract boundaries are trimmed to the extent of the overall study area, but not limited internally by clouds, unmodeled pixels, and excluded image artifacts. (For interpretation of the references to color in this figure legend, the reader is referred to the web version of this article.)

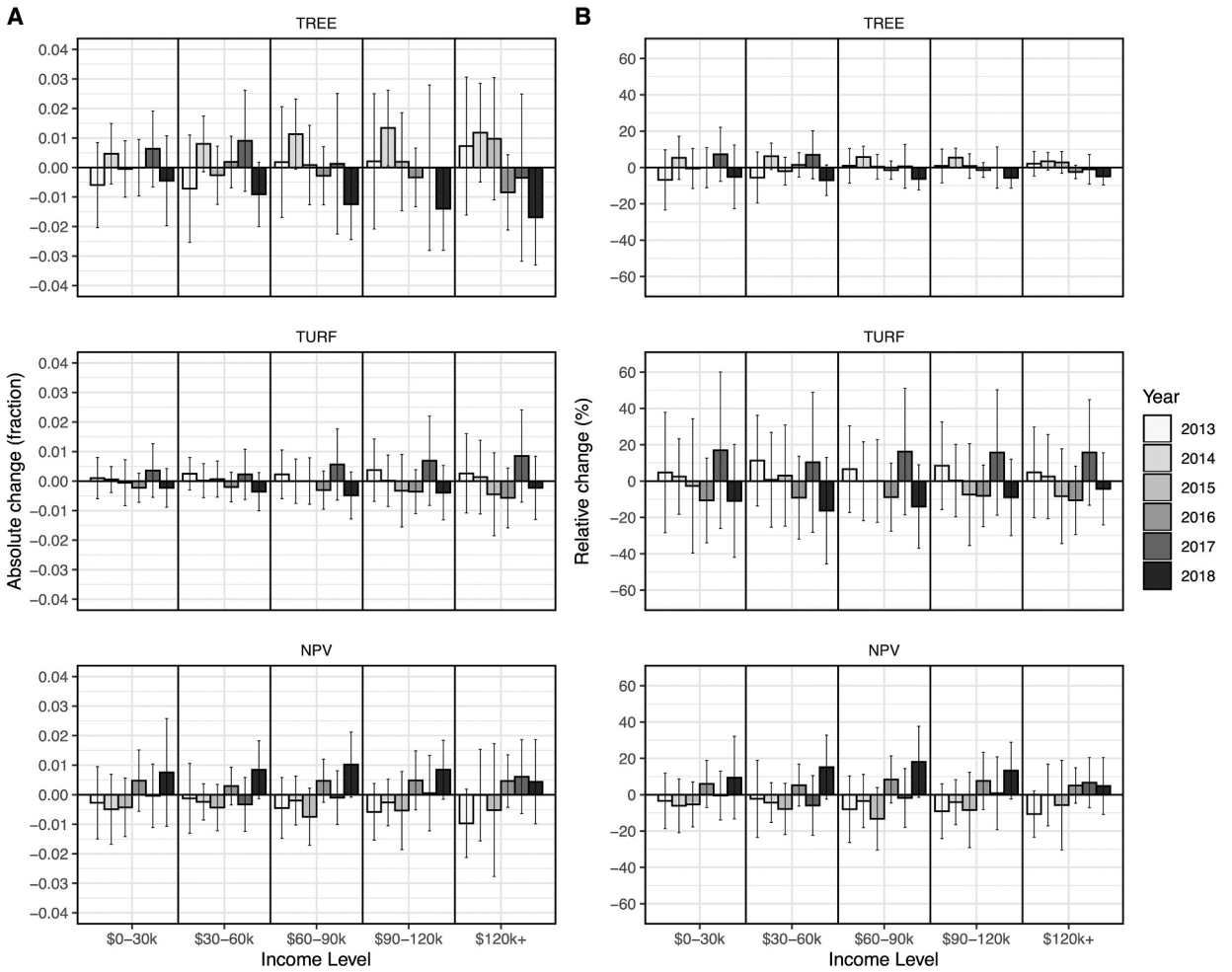

Fig. 5. Vegetation cover change across income levels. (A) Left column, mean absolute change anomalies (fractions) from mean of time series of vegetation cover types. (B) Right column, mean relative change anomalies (%) from mean of time series of vegetation cover types. Error bars are ±1 SD from the census tracts, weighted by number of pixels in each census tract.

consistent trend with most income levels showing a general decrease in turfgrass cover over time, except for high values in 2017. The magnitude in year-to-year adjustments in turfgrass cover was also greater for higher income levels than for lower income levels. All income levels had relatively higher NPV cover in 2016 and 2018 than other years. Higher income levels did not necessarily have greater increases in NPV than the other income levels, in contrast to the greater shifts for higher income bins observed for trees and turfgrass. However, when scaled relative to the mean vegetation cover fraction for the entire time series, differences in the magnitude of cover change between income levels were no longer as apparent for tree and turfgrass cover types (Fig. 5B). For trees, the higher income levels did not have relatively more change than the lower income bins. In fact, many of the lower income bins had relatively similar changes through time (except for estimates in 2013), while the highest income level, >$120 k, had relatively smaller changes, likely due to its much higher baseline of tree cover. Relative changes in turfgrass were very similar throughout the time series and appeared to be largely independent of income level. NPV cover changes had very similar temporal patterns after normalizing for mean cover as they did for absolute fractional cover changes, and the greatest increases in NPV in 2018 relative to the mean were still in the middle income levels. Although the proportions of vegetation cover types varied by median household income, the vegetation cover proportions within each income level remained relatively constant through all years of the time series (Fig. S15). There were small year-to-year changes in vegetation cover estimates but these did not amount to dramatic changes in cover by median household income level in aggregate as the drought progressed.

3.2.2. Outdoor water use

After estimating typical single-family residential mean outdoor water use per household from an average rainfall year (2006), we considered outdoor water usage in the following quintile bins, in units of m^3/household: very low (0–2.77), low (2.77–6.63), medium (6.63–15.71), high (15.71–24.54), and very high (24.54–588.99). This meant the highest outdoor water users used up to an order of magnitude more water than any of the other outdoor water use levels.

We compared the absolute fractional changes in vegetation cover types by level of outdoor water use (Fig. 6A). Tree cover changes in the high and very high water use levels showed more consistent year-over-year reductions through the time series than the lower water use levels. Turfgrass fractions were higher in 2013 than the mean of the time series for all water use levels. In general, higher water use levels showed greater variability in turfgrass than the lower water use levels. Year-to-year changes in NPV generally showed increases through the time series, but this was more apparent in the higher water use levels. When scaled to relative change by the mean of the time series (Fig. 6B), the overall temporal patterns in water use bins were similar to the observed shifts in absolute fraction totals. For trees, the relative magnitudes of changes were small for the higher water use levels. Relative turfgrass and NPV changes were of a similar magnitude across all water use levels. NPV values were greatest in 2018 for all water use levels. In general, overall vegetation cover increased with mean outdoor water use, and these proportions were largely stable through time (Fig. S16).

4. Discussion

4.1. Importance of separating urban vegetation types through time

We confirmed distinct temporal responses of different types of urban vegetation to drought at the metropolitan scale. This is especially important because of the effects that different types of healthy vegetation cover can have on local urban climates (e.g., Norton et al., 2015). For example, turfgrass lawns have greater evapotranspiration rates than trees and provide significant cooling through latent heat loss (Liang et al., 2017; Wheeler et al., 2019), and evapotranspiration rates can depend on whether the land use is residential or recreational (Peters et al., 2011). Tree evapotranspiration is highly variable by species (Pataki et al., 2011) and can significantly reduce air temperatures in areas with large amounts of tree cover (Wang et al., 2017; Ziter et al., 2019; Alonzo et al., 2021); at very local scales, shading from tree cover is often a far more influential moderator of air and surface temperatures (Souch and

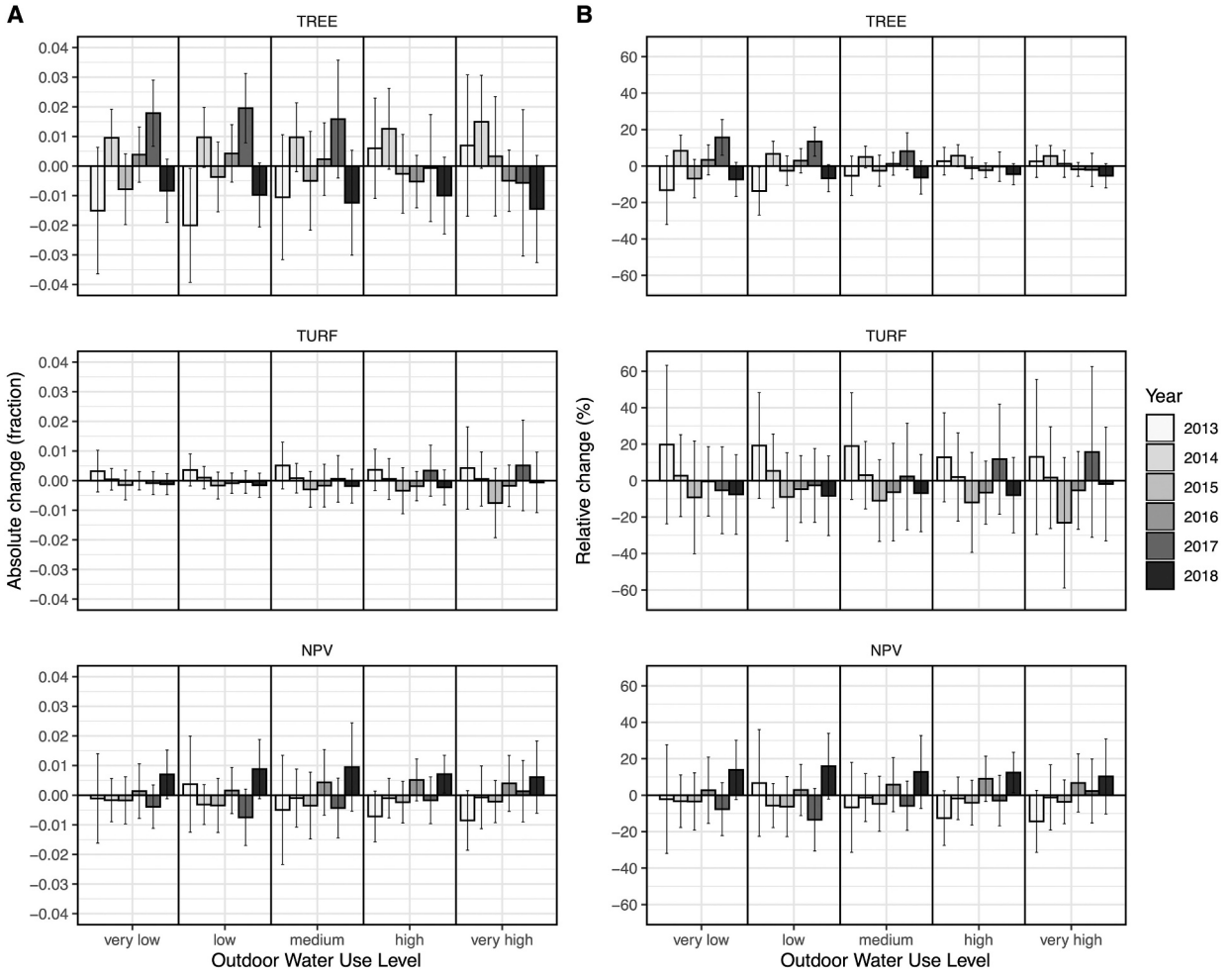

Fig. 6. Change in vegetation cover across outdoor water use levels. (A) Left column, mean absolute change anomalies (fractions) from mean of time series of vegetation cover types. (B) Right column, mean relative change anomalies (%) from mean of time series of vegetation cover types. Error bars are ±1 SD from the postal carrier routes, weighted by number of pixels in each postal carrier route.

Souch, 1993). Although not actively photosynthesizing, NPV-covered areas represent seasonal contributors of latent exchange during wetter seasons or months in contrast to non-vegetated surfaces which, with the exception of bare soil, are unlikely to return to vegetated cover (Pincetl et al., 2019).

We mapped fractional cover estimates of different types of urban vegetation from a multi-annual time series of airborne imaging spectroscopy data. Other urban remote sensing studies have tracked trees and/or turfgrass through time (e.g., Gillespie et al., 2012; Hedblom et al., 2017; Allen et al., 2021), but to our knowledge this is the first study to separately track trees, turfgrass, and NPV cover through time across a large metropolitan region. Overall, our cover estimates (mean values: tree = 0.20, turfgrass = 0.03, NPV = 0.06; Table 2) are comparable to those measured for a single point in time in other recent studies in the Los Angeles area during summer (McPherson et al., 2011; Wetherley et al., 2018), despite differences in year and month of acquisitions (Los Angeles city: tree/shrub = 0.21, irrigated grass = 0.12, dry grass/soil = 0.06, McPherson et al., 2011; Los Angeles metropolitan area: tree = 0.20, turfgrass = 0.04, NPV = 0.07, Wetherley et al., 2018).

4.2. Impacts of drought on urban vegetation and implications for urban climate of Los Angeles

The different long-term drought responses observed between urban vegetation types were likely related to both physiological differences as well as trending changes in outdoor water use over the duration of the event (Peters et al., 2011; McPherson et al., 2011; Wheeler et al., 2019). Overall, turfgrass cover declined and NPV cover increased between 2013 and 2018. We observed turfgrass to be highly sensitive to winter rainfall, recovering during wetter years such as 2017 and rapidly reverting to NPV in 2018. Although turfgrass in 2018 may have been primed for senescence after many years of drought, we hypothesize that this quick return of NPV may have been exacerbated by water conservation measures (Los Angeles Department of Water and Power, 2017). Water use reduction targets were implemented throughout the city during the 2012–2016 drought, with continued reductions planned into 2035 (Los Angeles Department of Water and Power, 2017; Palazzo et al., 2017).

In contrast to turfgrass, mean tree cover did not exhibit any large changes for most of the time series, with major reductions occurring only in 2018 after the main drought had ended. This observed aggregate decline is supported by other studies that have quantified larger declines in trees after a drought has ended, due to accumulated stress and weakened health (Trugman et al., 2018; Kannenberg et al., 2020). While extensive drought-driven tree mortality has been observed in natural areas in California such as the Sierra Nevada mountains (Fettig et al., 2019), the lack of significant reductions in our study implies that urban tree mortality was less widespread during the study period. Despite this, canopy loss and deaths of individual urban trees were documented throughout the southern California region but rarely at the scale of entire tree stands (Stevens et al., 2015; Miller et al., 2020). Confirming mortality estimation would require higher spatial resolution imagery, in which individual trees could be uniquely tracked, or repeated field surveys.

At the neighborhood scale, drought impacts depended on the amount and type of local vegetation cover. The relative proportions of different vegetation cover types shifted based on the overall amount of vegetation cover (Fig. 3), affecting the available ecosystem services that are provided by trees versus turfgrass. Tree cover largely persisted, and continued to provide shade and evaporative cooling; thus tree-dominated neighborhoods remained more resilient against urban heating during the drought. Conversely, turfgrass rapidly senesced so neighborhoods dominated by turfgrass were less resilient, and likely felt the additional heating impacts of the drought more acutely (Allen et al., 2021). As a consequence, our results imply that spatial distributions of trees versus turfgrass, as presented here, may be more informative for quantifying vegetation climate impacts during drought compared to a generic 'urban green vegetation cover' classification (e.g., Franke et al., 2009; McPherson et al., 2011; Degerickx et al., 2020).

4.3. Effects of physiography, income, and water use

The dynamic changes in turfgrass, NPV, and tree cover showed unique patterns relative to large scale physiographic features. Turfgrass loss was concentrated in the inland valleys in the north (San Fernando Valley) and east (San Gabriel Valley) of the study area, which tend to be warmer and drier than the Los Angeles Basin (Tayyebi and Jenerette, 2016; Crum et al., 2017; Pincetl et al., 2019). Thus, preferential turfgrass loss might be expected. However, corresponding NPV cover gains were not as pronounced in these regions, suggesting greater conversion to non-vegetated urban surfaces—at the time, widespread lawn removal programs were instituted in these areas to reduce irrigation demand (Pincetl et al., 2019). Instead, NPV cover gains were more prominent in hilly and mountainous areas with varied terrain, which correspond to more limited urban development and lower population densities. Tree cover changes were less geographically concentrated and were likely influenced by local factors that determined tree cover distribution initially, such as time of urban development, land parcel size, or socioeconomic conditions (Gillespie et al., 2012; Pincetl et al., 2013a; Pincetl et al., 2013b).

High income households proved more adaptable and resilient to drought conditions while also exhibiting greater absolute year-to-year changes in tree and turfgrass cover (Fig. 5A). This apparent contradiction is because higher income areas had larger amounts of vegetation cover prior to drought (thus more to lose overall), but at the same time residents could more effectively support existing vegetation cover (Pincetl et al., 2019). In contrast, middle-income areas, which began with significant vegetation cover but ultimately had fewer resources to maintain it during sustained drought, often experienced similar or greater relative losses of turfgrass compared to higher income neighborhoods (Fig. 5B). Although it was beyond the scope of our analysis for this study, the climate benefits resulting from more effective vegetation maintenance throughout the drought would be one of several contributing factors to greater drought resiliency for high income residents, including access to air conditioning (Schwarz et al., 2015; Fraser et al., 2017; Palazzo et al., 2017). While many studies have investigated the relationship between vegetation or tree cover and income (Mini et al., 2014;

Schwarz et al., 2015; Tayyebi and Jenerette, 2016), few have examined this linkage between vegetation cover types and the health and resiliency of residents of different income levels during drought.

When organized into classes of typical (non-drought) outdoor water use, the degree to which year-to-year cover changes responded to the drought varied by vegetation type (Fig. 6). Tree cover in areas with typically high water use declined more consistently from 2013 to 2018 than did tree cover in areas with lower water use. A confounding factor may be that trees in high water use areas tended to occur in larger urban forest patches, and therefore changes in cover could be detected more consistently in 18 m spatial resolution imagery compared to isolated or more dispersed trees (more typical of low water use areas) which would only appear in subpixel mixtures (Herold et al., 2004). We detected the opposite trend for turfgrass, with lower water use areas showing greater relative reductions in turfgrass overall while high water use areas had greater year-to-year variability. This suggests that the drought had a more lasting effect on the turfgrass cover of lower water use areas, and may indicate more water conservation by lower water users compared to high water users (Palazzo et al., 2017). By extension, the climate benefits conferred by vegetation would be reduced more greatly in lower water use areas during drought, leaving lower income or more vulnerable populations at increased risk during extreme heat events (Tayyebi and Jenerette, 2016; Hulley et al., 2019; Schell et al., 2020).

4.4. Longer term implications of droughts for urban areas and vegetation

We observed rapid (turfgrass) and long-term (tree) cover changes over the course of our time series. Critically, because urban trees may take several years to exhibit stress and canopy loss, impacts may not be easily perceptible from year-to-year during a drought before manifesting as permanent changes over the long-term. Understanding these impacts will require multi-decadal studies (Gillespie et al., 2012) to complement annual analyses. For urban planners and residents, the challenge of maintaining urban green vegetation cover in arid or semi-arid climates will continue to grow as water conservation targets become more restrictive (McPherson et al., 2018; Los Angeles Department of Water and Power, 2017; Porse et al., 2018). In Los Angeles, the focus will likely be on residential water conservation: the Los Angeles Department of Water and Power (2017) has estimated that residential areas have the greatest maximum cost-effective conservation potential for water savings by 2035 (90,000 acre-ft/yr; 111.0×10^6 m^3/yr), with much smaller amounts for commercial-institutional-industrial (46,000; 56.7×10^6) and city-owned (4000; 4.9×10^6) areas. As vegetation becomes more expensive or difficult to maintain, its loss may become permanent, such as the permanent transitions from turfgrass to non-vegetated surfaces we observed in the San Gabriel Valley. However, the active conversion from turfgrass to xeriscaping is expensive and is a luxury enjoyed by wealthier residents; lower income areas may only be able to afford to let turfgrass senesce (Pincetl et al., 2019). Further, to become established, drought-tolerant vegetation may require additional irrigation inputs: counterintuitively, it is often best to plant drought-tolerant vegetation when water is readily available rather than during a severe drought (Porse et al., 2018). In the long-term, replacing turfgrass with drought-tolerant native plants and xeriscaping will reduce water use, but it will also affect energy budgets as latent heat loss decreases and local temperatures increase (Vahmani and Ban-Weiss, 2016; Pincetl et al., 2019; Wetherley et al., 2021).

While Los Angeles and many other California cities are prototypical examples of drought-affected regions (Lund et al., 2018), drought can affect urban vegetation growth and structure in wetter climates as well (e.g., Chicago, Illinois; Bialecki et al., 2018) but on different time scales relative to Mediterranean climates (e.g., Melbourne, Australia; May et al., 2013). Drought impacts will also vary with the local vegetation species palettes within cities, affecting local responses and the likelihood of planting native species, even in wetter climates (Jenerette et al., 2016). In the longer term, and faced with the prospect of severe droughts influenced by climate change (Sun et al., 2015; Williams et al., 2015; Marvel et al., 2019), cities will need to plan for extreme drought conditions when selecting vegetation (Norton et al., 2015), especially in seasonally dry regions such as California (McPherson et al., 2018; Quesnel et al., 2019; Pincetl et al., 2019).

5. Conclusions

We showed how a multi-year drought can give rise to major changes in urban vegetation cover distributions, using the 2012–2016 drought in Los Angeles, California as a case study. We found that trees and turfgrass cover changes responded at different time scales to drought and showed differing magnitudes of response based on broad-scale patterns in urban climatology and physiography. First, turfgrass was highly responsive to drought due to reductions of both precipitation and irrigation as well as higher temperatures, whereas the responses of trees were more buffered and tree cover changes took years to develop, even after the main 2012–2016 California drought had ended. Second, we found that turfgrass cover losses were most apparent in the inland valleys of the study area, indicating that different climatological regions within the Los Angeles metropolitan area had different vegetation responses to drought. Our results suggest that cooler coastal areas may have more difficulty maintaining turfgrass cover if climate change causes them to become more climatological similar to the current warm inland areas. These spatially differentiated losses were not apparent for trees. Third, we found that areas of the city with the highest levels of income and outdoor water use experienced the greatest absolute changes in tree and turfgrass cover. Relative to their mean amount of existing vegetation cover, the lower-income and lower outdoor water use areas more often had the greatest tree cover changes, and turfgrass and NPV changes became more similar across all income and outdoor water use levels. Therefore, during future droughts we might expect the largest absolute changes in urban vegetation cover to be found in wealthier and more well-watered areas of the city. However, in relative terms, the drought impacts on vegetation are likely to be more similar or even relatively greater for lower income and water use areas. Our results demonstrate how studies of urban vegetation cover changes and climate impacts can benefit from finer-scale spatial and vegetation type distinctions to gain a more detailed picture of local climate and drought impacts within urban landscapes.

Declaration of Competing Interest

The authors declare that they have no known competing financial interests or personal relationships that could have appeared to influence the work reported in this paper.

Acknowledgements

This study was funded by a NASA Earth and Space Science Fellowship (80NSSC18K1325). Special thanks to Sarah Lundeen at the Jet Propulsion Laboratory for assistance in obtaining the AVIRIS image time series; the County of Los Angeles for many of the key GIS layers; and Susan Meerdink for spectral calibration code. We gratefully acknowledge Michael Allen for feedback on the figures; Rachel Torres and Mike Alonzo for fruitful discussions about water, drought, and urban trees; and the constructive reviewer comments which greatly improved the manuscript.

Appendix A. Supplementary data

Supplementary data to this article can be found online at https://doi.org/10.1016/j.uclim.2022.101157.

References

Abatzoglou, J.T., McEvoy, D.J., Redmond, K.T., 2017. The west wide drought tracker: drought monitoring at fine spatial scales. Bull. Am. Meteorol. Soc. 98, 1815–1820. https://doi.org/10.1175/bams-d-16-0193.1.

Allen, M.A., Roberts, D.A., McFadden, J.P., 2021. Reduced urban green cover and daytime cooling capacity during the 2012–2016 California drought. Urban Clim. 36, 100768 https://doi.org/10.1016/j.uclim.2020.100768.

Alonzo, M., Bookhagen, B., Roberts, D.A., 2014. Urban tree species mapping using hyperspectral and lidar data fusion. Remote Sens. Environ. 148, 70–83. https://doi.org/10.1016/j.rse.2014.03.018.

Alonzo, M., Baker, M.E., Gao, Y., Shandas, V., 2021. Spatial configuration and time of day impacts the magnitude of urban tree canopy cooling. Environ. Res. Lett. https://doi.org/10.1088/1748-9326/ac12f2.

Avolio, M.L., Pataki, D.E., Gillespie, T.W., Jenerette, G.D., McCarthy, H.R., Pincetl, S., Weller Clarke, L., 2015. Tree diversity in southern California's urban forest: the interacting roles of social and environmental variables. Front. Ecol. Evol. 3, 1–15. https://doi.org/10.3389/fevo.2015.00073.

Bialecki, M.B., Fahey, R.T., Scharenbroch, B., 2018. Variation in urban forest productivity and response to extreme drought across a large metropolitan region. Urban Ecosyst. 21, 157–169. https://doi.org/10.1007/s11252-017-0692-z.

Bijoor, N.S., McCarthy, H.R., Zhang, D., Pataki, D.E., 2012. Water sources of urban trees in the Los Angeles metropolitan area. Urban Ecosyst. 15, 195–214. https://doi.org/10.1007/s11252-011-0196-1.

Cadenasso, M.L., Pickett, S.T.A., Schwarz, K., 2007. Spatial heterogeneity in urban ecosystems: reconceptualizing land cover and a framework for classification. Front. Ecol. Environ. 5, 80–88. https://doi.org/10.1890/1540-9295(2007)5[80:SHIUER]2.0.CO;2.

Cawse-Nicholson, K., Townsend, P.A., Schimel, D., Assiri, A.M., Blake, P.L., Buongiorno, M.F., Campbell, P., Carmon, N., Casey, K.A., Correa-Pabón, R.E., Dahlin, K. M., Dashti, H., Dennison, P.E., Dierssen, H., Erickson, A., Fisher, J.B., Frouin, R., Gatebe, C.K., Gholizadeh, H., Gierach, M., Glenn, N.F., Goodman, J.A., Griffith, D.M., Guild, L., Hakkenberg, C.R., Hochberg, E.J., Holmes, T.R.H., Hu, C., Hulley, G., Huemmrich, K.F., Kudela, R.M., Kokaly, R.F., Lee, C.M., Martin, R., Miller, C.E., Moses, W.J., Muller-Karger, F.E., Ortiz, J.D., Otis, D.B., Pahlevan, N., Painter, T.H., Pavlick, R., Poulter, B., Qi, Y., Realmuto, V.J., Roberts, D., Schaepman, M.E., Schneider, F.D., Schwandner, F.M., Serbin, S.P., Shiklomanov, A.N., Stavros, E.N., Thompson, D.R., Torres-Perez, J.L., Turpie, K.R., Tzortziou, M., Ustin, S., Yu, Q., Yusup, Y., Zhang, Q., 2021. NASA's surface biology and geology designated observable: a perspective on surface imaging algorithms. Remote Sens. Environ. 257, 112349 https://doi.org/10.1016/j.rse.2021.112349.

Chen, Y.J., McFadden, J.P., Clarke, K.C., Roberts, D.A., 2015. Measuring Spatio-temporal trends in residential landscape irrigation extent and rate in Los Angeles, California using SPOT-5 satellite imagery. Water Resour. Manag. 29, 5749–5763. https://doi.org/10.1007/s11269-015-1144-2.

Clarke, L.W., Jenerette, G.D., Davila, A., 2013. The luxury of vegetation and the legacy of tree biodiversity in Los Angeles, CA. Landsc. Urban Plan. 116, 48–59. https://doi.org/10.1016/j.landurbplan.2013.04.006.

County of Los Angeles, 2020. Median Household Income by Census Tract [WWW Document]. URL https://egis-lacounty.hub.arcgis.com/datasets/median-household-income-by-census-tract (accessed 9.22.20).

Crum, S.M., Shiflett, S.A., Jenerette, G.D., 2017. The influence of vegetation, mesoclimate and meteorology on urban atmospheric microclimates across a coastal to desert climate gradient. J. Environ. Manag. 200, 295–303. https://doi.org/10.1016/j.jenvman.2017.05.077.

Czekajlo, A., Coops, N.C., Wulder, M.A., Hermosilla, T., Lu, Y., White, J.C., van den Bosch, M., 2020. The urban greenness score: a satellite-based metric for multi-decadal characterization of urban land dynamics. Int. J. Appl. Earth Obs. Geoinf. 93, 102210 https://doi.org/10.1016/j.jag.2020.102210.

Davis, M., 2006. City of Quartz: Excavating the Future in Los Angeles, New edition. Verso Books.

Degerickx, J., Hermy, M., Somers, B., 2020. Mapping functional urban green types using high resolution remote sensing data. Sustainability 12, 2144. https://doi.org/10.3390/su12052144.

Demuzere, M., Orru, K., Heidrich, O., Olazabal, E., Geneletti, D., Orru, H., Bhave, A.G., Mittal, N., Feliu, E., Faehnle, M., 2014. Mitigating and adapting to climate change: multi-functional and multi-scale assessment of green urban infrastructure. J. Environ. Manag. 146, 107–115. https://doi.org/10.1016/j.jenvman.2014.07.025.

Dennison, P.E., Roberts, D.A., 2003. Endmember selection for multiple endmember spectral mixture analysis using endmember average RMSE. Remote Sens. Environ. 87, 123–135. https://doi.org/10.1016/S0034-4257(03)00135-4.

Dennison, P.E., Qi, Y., Meerdink, S.K., Kokaly, R.F., Thompson, D.R., Daughtry, C.S.T., Quemada, M., Roberts, D.A., Gader, P.D., Wetherley, E.B., Numata, I., Roth, K. L., 2019. Comparison of methods for modeling fractional cover using simulated satellite hyperspectral imager spectra. Remote Sens. 11, 2072. https://doi.org/10.3390/rs11182072.

Erker, T., Wang, L., Lorentz, L., Stoltman, A., Townsend, P.A., 2019. A statewide urban tree canopy mapping method. Remote Sens. Environ. 229, 148–158. https://doi.org/10.1016/j.rse.2019.03.037.

Fettig, C.J., Mortenson, L.A., Bulaon, B.M., Foulk, P.B., 2019. Tree mortality following drought in the central and southern Sierra Nevada, California, U.S. For. Ecol. Manag. 432, 164–178. https://doi.org/10.1016/j.foreco.2018.09.006.

Franke, J., Roberts, D.A., Halligan, K., Menz, G., 2009. Hierarchical Multiple Endmember Spectral Mixture Analysis (MESMA) of hyperspectral imagery for urban environments. Remote Sens. Environ. 113, 1712–1723. https://doi.org/10.1016/j.rse.2009.03.018.

Fraser, A.M., Chester, M.V., Eisenman, D., Hondula, D.M., Pincetl, S.S., English, P., Bondank, E., 2017. Household accessibility to heat refuges: residential air conditioning, public cooled space, and walkability. Environ. Plan. B Urban Anal. City Sci. 44, 1036–1055. https://doi.org/10.1177/0265813516657342.

Gillespie, T.W., Pincetl, S., Brossard, S., Smith, J., Saatchi, S., Pataki, D., Saphores, J.-D., 2012. A time series of urban forestry in Los Angeles. Urban Ecosyst. 15, 233–246. https://doi.org/10.1007/s11252-011-0183-6.

Green, R.O., Eastwood, M.L., Sarture, C.M., Chrien, T.G., Aronsson, M., Chippendale, B.J., Faust, J.A., Pavri, B.E., Chovit, C.J., Solis, M., Olah, M.R., Williams, O., 1998. Imaging spectroscopy and the Airborne Visible/Infrared Imaging Spectrometer (AVIRIS). Remote Sens. Environ. 65, 227–248. https://doi.org/10.1016/S0034-4257(98)00064-9.

Hedblom, M., Lindberg, F., Vogel, E., Wissman, J., Ahrné, K., 2017. Estimating urban lawn cover in space and time: case studies in three Swedish cities. Urban Ecosyst. 20, 1109–1119. https://doi.org/10.1007/s11252-017-0658-1.

Herold, M., Roberts, D.A., Gardner, M.E., Dennison, P.E., 2004. Spectrometry for urban area remote sensing – development and analysis of a spectral library from 350 to 2400 nm. Remote Sens. Environ. 91, 304–319. https://doi.org/10.1016/j.rse.2004.02.013.

Hulley, G., Shivers, S., Wetherley, E., Cudd, R., 2019. New ECOSTRESS and MODIS land surface temperature data reveal fine-scale heat vulnerability in cities: a case study for Los Angeles County, California. Remote Sens. 11, 6–8. https://doi.org/10.3390/rs11182136.

Jenerette, G.D., Clarke, L.W., Avolio, M.L., Pataki, D.E., Gillespie, T.W., Pincetl, S., Nowak, D.J., Hutyra, L.R., McHale, M., McFadden, J.P., Alonzo, M., 2016. Climate tolerances and trait choices shape continental patterns of urban tree biodiversity. Glob. Ecol. Biogeogr. 25, 1367–1376. https://doi.org/10.1111/geb.12499.

Kannenberg, S.A., Schwalm, C.R., Anderegg, W.R.L., 2020. Ghosts of the past: how drought legacy effects shape forest functioning and carbon cycling. Ecol. Lett. https://doi.org/10.1111/ele.13485 ele.13485.

Kaplan, S., Myint, S.W., Fan, C., Brazel, A.J., 2014. Quantifying outdoor water consumption of urban land use/land cover: sensitivity to drought. Environ. Manag. 53, 855–864. https://doi.org/10.1007/s00267-014-0245-7.

Kaufmann, J.E., 1994. Principles of turfgrass growth and development. In: Leslie, A.R. (Ed.), Handbook of Integrated Pest Management for Turf and Ornamentals, pp. 91–98. Lewis, USA.

Lee, C.M., Cable, M.L., Hook, S.J., Green, R.O., Ustin, S.L., Mandl, D.J., Middleton, E.M., 2015. An introduction to the NASA Hyperspectral InfraRed Imager (HyspIRI) mission and preparatory activities. Remote Sens. Environ. 167, 6–19. https://doi.org/10.1016/j.rse.2015.06.012.

Liang, L.L., Anderson, R.G., Shiflett, S.A., Jenerette, G.D., 2017. Urban outdoor water use and response to drought assessed through mobile energy balance and vegetation greenness measurements. Environ. Res. Lett. 12 https://doi.org/10.1088/1748-9326/aa7b21.

Litvak, E., Manago, K.F., Hogue, T.S., Pataki, D.E., 2017. Evapotranspiration of urban landscapes in Los Angeles, California at the municipal scale. Water Resour. Res. 53, 4236–4252. https://doi.org/10.1002/2016WR020254.

Liu, L., Coops, N.C., Aven, N.W., Pang, Y., 2017. Mapping urban tree species using integrated airborne hyperspectral and LiDAR remote sensing data. Remote Sens. Environ. 200, 170–182. https://doi.org/10.1016/j.rse.2017.08.010.

Los Angeles Department of Water and Power, 2017. Executive Report Water Conservation Potential Study.

Lund, J., Medellin-Azuara, J., Durand, J., Stone, K., 2018. Lessons from California's 2012–2016 drought. J. Water Resour. Plan. Manag. 144, 04018067. https://doi.org/10.1061/(asce)wr.1943-5452.0000984.

Marchionni, V., Fatichi, S., Tapper, N., Walker, J.P., Manoli, G., Daly, E., 2021. Assessing vegetation response to irrigation strategies and soil properties in an urban reserve in Southeast Australia. Landsc. Urban Plan. 215, 104198 https://doi.org/10.1016/j.landurbplan.2021.104198.

Marvel, K., Cook, B.I., Bonfils, C.J.W., Durack, P.J., Smerdon, J.E., Williams, A.P., 2019. Twentieth-century hydroclimate changes consistent with human influence. Nature 569, 59–65. https://doi.org/10.1038/s41586-019-1149-8.

May, P.B., Livesley, S.J., Shears, I., 2013. Managing and monitoring tree health and soil water status during extreme drought in Melbourne, Victoria. Arboric. Urban For. 39, 136–145.

McPherson, E.G., Simpson, J.R., Xiao, Q.F., Wu, C.X., 2011. Million trees Los Angeles canopy cover and benefit assessment. Landsc. Urban Plan. 99, 40–50.

McPherson, E.G., Berry, A.M., van Doorn, N.S., 2018. Performance testing to identify climate-ready trees. Urban For. Urban Green. 29, 28–39. https://doi.org/10.1016/j.ufug.2017.09.003.

Miller, D.L., Alonzo, M., Roberts, D.A., Tague, C.L., McFadden, J.P., 2020. Drought response of urban trees and turfgrass using airborne imaging spectroscopy. Remote Sens. Environ. 240, 111646 https://doi.org/10.1016/j.rse.2020.111646.

Miller, D.L., Alonzo, M., Meerdink, S.K., Allen, M.A., Tague, C.L., Roberts, D.A., McFadden, J.P., 2022. Seasonal and interannual drought responses of vegetation in a California urbanized area measured using complementary remote sensing indices. ISPRS J. Photogramm. Remote Sens. 183, 178–195. https://doi.org/10.1016/j.isprsjprs.2021.11.002.

Mini, C., Hogue, T.S., Pincetl, S., 2014. Estimation of residential outdoor water use in Los Angeles, California. Landsc. Urban Plan. 127, 124–135. https://doi.org/10.1016/j.landurbplan.2014.04.007.

Moskal, L.M., Styers, D.M., Halabisky, M., 2011. Monitoring urban tree cover using object-based image analysis and public domain remotely sensed data. Remote Sens. 3, 2243–2262. https://doi.org/10.3390/rs3102243.

National Centers for Environmental Information, 2020. Data Tools: 1981-2010 Normals, Los Angeles Downtown USC, CA US [WWW Document]. URL https://www.ncdc.noaa.gov/cdo-web/datatools/normals (accessed 11.5.20).

Norton, B.A., Coutts, A.M., Livesley, S.J., Harris, R.J., Hunter, A.M., Williams, N.S.G., 2015. Planning for cooler cities: a framework to prioritise green infrastructure to mitigate high temperatures in urban landscapes. Landsc. Urban Plan. 134, 127–138. https://doi.org/10.1016/j.landurbplan.2014.10.018.

O'Neil-Dunne, J., MacFaden, S., Royar, A., 2014. A versatile, production-oriented approach to high-resolution tree-canopy mapping in urban and suburban landscapes using GEOBIA and data fusion. Remote Sens. 6, 12837–12865. https://doi.org/10.3390/rs61212837.

Palazzo, J., Liu, O.R., Stillinger, T., Song, R., Wang, Y., Hiroyasu, E.H.T., Zenteno, J., Anderson, S., Tague, C., 2017. Urban responses to restrictive conservation policy during drought. Water Resour. Res. 53, 4459–4475. https://doi.org/10.1002/2016WR020136.

Palmer, W.C., 1965. Meteorological Drought. US Department of Commerce, Weather Bureau.

Pataki, D.E., Boone, C.G., Hogue, T.S., Jenerette, G.D., McFadden, J.P., Pincetl, S., 2011. Socio-ecohydrology and the urban water challenge. Ecohydrology 4, 341–347. https://doi.org/10.1002/eco.209.

Peters, E.B., Hiller, R.V., McFadden, J.P., 2011. Seasonal contributions of vegetation types to suburban evapotranspiration. J. Geophys. Res. Biogeosci. 116, 1–16. https://doi.org/10.1029/2010JG001463.

Pincetl, S., Gillespie, T., Pataki, D.E., Saatchi, S., Saphores, J.-D., 2013a. Urban tree planting programs, function or fashion? Los Angeles and urban tree planting campaigns. GeoJournal 78, 475–493. https://doi.org/10.1007/s10708-012-9446-x.

Pincetl, S., Prabhu, S.S., Gillespie, T.W., Jenerette, G.D., Pataki, D.E., 2013b. The evolution of tree nursery offerings in Los Angeles County over the last 110 years. Landsc. Urban Plan. 118, 10–17. https://doi.org/10.1016/j.landurbplan.2013.05.002.

Pincetl, S., Gillespie, T.W., Pataki, D.E., Porse, E., Jia, S., Kidera, E., Nobles, N., Rodriguez, J., Choi, D., 2019. Evaluating the effects of turf-replacement programs in Los Angeles. Landsc. Urban Plan. 185, 210–221. https://doi.org/10.1016/j.landurbplan.2019.01.011.

Porse, E., Mika, K.B., Litvak, E., Manago, K.F., Hogue, T.S., Gold, M., Pataki, D.E., Pincetl, S., 2018. The economic value of local water supplies in Los Angeles. Nat. Sustain. 1, 289–297. https://doi.org/10.1038/s41893-018-0068-2.

Quesnel, K.J., Ajami, N., Marx, A., 2019. Shifting landscapes: decoupled urban irrigation and greenness patterns during severe drought. Environ. Res. Lett. 14, 064012 https://doi.org/10.1088/1748-9326/ab20d4.

Reyes, B., Hogue, T.S., Maxwell, R.M., 2020. Urban irrigation in the modeling of a semi-arid urban environment: Ballona Creek watershed, Los Angeles, California. Hydrol. Sci. J. 65, 1344–1357. https://doi.org/10.1080/02626667.2020.1751846.

Richards, D.R., Passy, P., Oh, R.R.Y., 2017. Impacts of population density and wealth on the quantity and structure of urban green space in tropical Southeast Asia. Landsc. Urban Plan. 157, 553–560. https://doi.org/10.1016/j.landurbplan.2016.09.005.

Roberts, D.A., Gardner, M., Church, R., Ustin, S., Scheer, G., 1998. Mapping chaparral in the Santa Monica Mountains using multiple endmember spectral mixture models. Remote Sens. Environ. 65, 267–279. https://doi.org/10.1016/S0034-4257(98)00037-6.

Roberts, D.A., Halligan, K., Dennison, P., Dudley, K., Somers, B., Crabbe, A., 2019. A Viper Tools User Manual, Version 2.1.

Roman, L.A., Pearsall, H., Eisenman, T.S., Conway, T.M., Fahey, R.T., Landry, S., Vogt, J., van Doorn, N.S., Grove, J.M., Locke, D.H., Bardekjian, A.C., Battles, J.J., Cadenasso, M.L., van den Bosch, C.C.K., Avolio, M., Berland, A., Jenerette, G.D., Mincey, S.K., Pataki, D.E., Staudhammer, C., 2018. Human and biophysical legacies shape contemporary urban forests: a literature synthesis. Urban For. Urban Green. 31, 157–168. https://doi.org/10.1016/j.ufug.2018.03.004.

Savi, T., Bertuzzi, S., Branca, S., Tretiach, M., Nardini, A., 2015. Drought-induced xylem cavitation and hydraulic deterioration: risk factors for urban trees under climate change? New Phytol. 205, 1106–1116. https://doi.org/10.1111/nph.13112.

Schell, C.J., Dyson, K., Fuentes, T.L., Roches, S. Des, Harris, N.C., Miller, D.S., Woelfle-Erskine, C.A., Lambert, M.R., 2020. The ecological and evolutionary consequences of systemic racism in urban environments. Science (80-.) 369. https://doi.org/10.1126/SCIENCE.AAY4497.

Schug, F., Frantz, D., Okujeni, A., van der Linden, S., Hostert, P., 2020. Mapping urban-rural gradients of settlements and vegetation at national scale using Sentinel-2 spectral-temporal metrics and regression-based unmixing with synthetic training data. Remote Sens. Environ. 246, 111810 https://doi.org/10.1016/j.rse.2020.111810.

Schwarz, K., Fragkias, M., Boone, C.G., Zhou, W., McHale, M., Grove, J.M., O'Neil-Dunne, J., McFadden, J.P., Buckley, G.L., Childers, D., Ogden, L., Pincetl, S., Pataki, D., Whitmer, A., Cadenasso, M.L., 2015. Trees grow on money: urban tree canopy cover and environmental justice. PLoS One 10. https://doi.org/10.1371/journal.pone.0122051 e0122051.

Souch, C.A., Souch, C., 1993. The effect of trees on summertime below canopy urban climates: a case study Bloomington, Indiana. J. Arboric. 19, 303–312.

Stevens, M., Goldenstein, T., Perry, T., 2015. Dying trees may force new outlook on irrigation during drought [WWW Document]. Los Angeles Times. URL https://www.latimes.com/local/california/la-me-drought-trees-20150612-story.html (accessed 11.29.20).

Sun, F., Walton, D.B., Hall, A., 2015. A hybrid dynamical-statistical downscaling technique. Part II: end-of-century warming projections predict a new climate state in the Los Angeles region. J. Clim. 28, 4618–4636. https://doi.org/10.1175/JCLI-D-14-00197.1.

Tayyebi, A., Jenerette, G.D., 2016. Increases in the climate change adaption effectiveness and availability of vegetation across a coastal to desert climate gradient in metropolitan Los Angeles, CA, USA. Sci. Total Environ. 548–549, 60–71. https://doi.org/10.1016/j.scitotenv.2016.01.049.

Thompson, D.R., Gao, B.C., Green, R.O., Roberts, D.A., Dennison, P.E., Lundeen, S.R., 2015. Atmospheric correction for global mapping spectroscopy: ATREM advances for the HyspIRI preparatory campaign. Remote Sens. Environ. 167, 64–77. https://doi.org/10.1016/j.rse.2015.02.010.

Trugman, A.T., Detto, M., Bartlett, M.K., Medvigy, D., Anderegg, W.R.L., Schwalm, C., Schaffer, B., Pacala, S.W., 2018. Tree carbon allocation explains forest drought-kill and recovery patterns. Ecol. Lett. 21, 1552–1560. https://doi.org/10.1111/ele.13136.

US Census Bureau, 2010. 2010 US Census Demographic Profile (Vector Digital Data) [WWW Document]. URL. http://www.census.gov/geo/maps-data/data/tiger.html.

US Census Bureau, 2020. QuickFacts Los Angeles County, California [WWW Document]. URL. https://www.census.gov/quickfacts/losangelescountycalifornia.

Vahmani, P., Ban-Weiss, G., 2016. Climatic consequences of adopting drought-tolerant vegetation over Los Angeles as a response to California drought. Geophys. Res. Lett. 43, 8240–8249. https://doi.org/10.1002/2016GL069658.

van der Linden, S., Okujeni, A., Canters, F., Degerickx, J., Heiden, U., Hostert, P., Priem, F., Somers, B., Thiel, F., 2018. Imaging spectroscopy of urban environments. Surv. Geophys. https://doi.org/10.1007/s10712-018-9486-y.

Vicente-Serrano, S.M., Beguería, S., López-Moreno, J.I., 2010. A multiscalar drought index sensitive to global warming: the standardized precipitation evapotranspiration index. J. Clim. 23, 1696–1718. https://doi.org/10.1175/2009JCLI2909.1.

Wang, J.A., Hutyra, L.R., Li, D., Friedl, M.A., 2017. Gradients of atmospheric temperature and humidity controlled by local urban land-use intensity in Boston. J. Appl. Meteorol. Climatol. 56, 817–831. https://doi.org/10.1175/JAMC-D-16-0325.1.

Wetherley, E.B., Roberts, D.A., McFadden, J.P., 2017. Mapping spectrally similar urban materials at sub-pixel scales. Remote Sens. Environ. 195, 170–183. https://doi.org/10.1016/j.rse.2017.04.013.

Wetherley, E.B., McFadden, J.P., Roberts, D.A., 2018. Megacity-scale analysis of urban vegetation temperatures. Remote Sens. Environ. 213, 18–33. https://doi.org/10.1016/j.rse.2018.04.051.

Wetherley, E.B., Roberts, D.A., Tague, C.L., Jones, C., Quattrochi, D.A., McFadden, J.P., 2021. Remote sensing and energy balance modeling of urban climate variability across a semi-arid megacity. Urban Clim. 35, 100757 https://doi.org/10.1016/j.uclim.2020.100757.

Wheeler, S.M., Abunnasr, Y., Dialesandro, J., Assaf, E., Agopian, S., Gamberini, V.C., 2019. Mitigating urban heating in dryland cities: a literature review. J. Plan. Lit. 34, 434–446. https://doi.org/10.1177/0885412219855779.

Williams, A.P., Seager, R., Abatzoglou, J., Cook, B., Smerdon, J., Cook, E., 2015. Contribution of anthropogenic warming to California drought during 2012–2014. Geophys. Res. Lett. 1–10. https://doi.org/10.1002/2015GL064924.Received.

Winguth, A.M.E., Kelp, B., 2013. The urban heat island of the north-central Texas region and its relation to the 2011 severe Texas drought. J. Appl. Meteorol. Climatol. 52, 2418–2433. https://doi.org/10.1175/JAMC-D-12-0195.1.

Wolch, J.R., Byrne, J., Newell, J.P., 2014. Urban green space, public health, and environmental justice: the challenge of making cities 'just green enough'. Landsc. Urban Plan. 125, 234–244. https://doi.org/10.1016/j.landurbplan.2014.01.017.

Zhao, L., Oleson, K., Bou-Zeid, E., Krayenhoff, E.S., Bray, A., Zhu, Q., Zheng, Z., Chen, C., Oppenheimer, M., 2021. Global multi-model projections of local urban climates. Nat. Clim. Chang. 11 https://doi.org/10.1038/s41558-020-00958-8.

Ziter, C.D., Pedersen, E.J., Kucharik, C.J., Turner, M.G., 2019. Scale-dependent interactions between tree canopy cover and impervious surfaces reduce daytime urban heat during summer. Proc. Natl. Acad. Sci. https://doi.org/10.1073/pnas.1817561116, 201817561.